



UNIVERSIDAD AUTÓNOMA DE SINALOA
FACULTAD DE CIENCIAS DE LA TIERRA Y EL ESPACIO



BOLETÍN VOL. 7, NÚM. 2
OCTUBRE 2019

CONTÁCTANOS EN:



observatorio.facite@uas.edu.mx

PÁGINA WEB:



<http://facite.uas.edu.mx/observatorio/>



Boletín Vol. 7, Núm. 2 Octubre 2019

Contenido

ARTÍCULOS	1
Structural Health Monitoring of Bridges using GPS Technology	1
Utility of GNSS Radio Occultation technique for tropopause height investigation over Egypt	2
Shoreline monitoring by GNSS-PPP aiming to attendance the law 14.258/2010 from Pernambuco State, Brazil	3
Mapping Forest Landscape Multifunctionality Using Multicriteria Spatial Analysis	4
Spatial analysis on tuberculosis and the network of primary health care	5
Land use and water quality in watersheds in the State of São Paulo, based on GIS and SWAT data	5
Cleaning radio interferometric images using spherical descomposition	6
BeamModelTester: Software framework for testing radio telescope beams	7
NOTICIAS	8
CONGRESOS	9
PROGRAMA DE CONFERENCIAS Y TALLERES	10

Directorio

Dr. Juan Eulogio Guerra Liera

Rector

M.C. Jesús Madueña Molina

Secretario General

Dr. Wenseslao Plata Rocha

Director

M.C. Aníbal Israel Arana Medina

Secretario Académico

Ing. Jazive Rebeca Sánchez Jacobo

Coordinadora del Observatorio Infotecnológico



ARTÍCULOS: GEODESIA, GEOMÁTICA Y ASTRONOMÍA

Structural Health Monitoring of Bridges using GPS Technology

Gaxiola-Camacho, J., Vazquez-Becerra-G., Millan-Almaraz-J., Vazquez-Ontiveros, J., Lopez-Varelas, F. and Gaxiola-Camacho, O., (2019). *LABSE-SMIS 2nd Bridge Engineering Workshop Mexico 2019*.

Abstract

The use of GPS (Global Positioning System) technology in SHM (Structural Health Monitoring) started by the end of the eighties. However, its use in the SHM of bridges was reported in the middle of the nineties in the United States, Canada, and Europe. Thus, it can be considered as a relatively new research topic. This paper demonstrates the applicability of GPS in the SHM of bridges. The structural performance of the Juarez Bridge located in Culiacán, Mexico is studied using GPS receivers. An alternative technique is proposed to compute the structural reliability of bridges evaluating allowable deflections recommended by the American Association of State Highway and Transportation Officials (AASHTO) Bridge Construction Manual. Based on the results presented in this paper, the proposed methodology represents an alternative for extracting safety information of bridges using GPS technology.



Figure 1. The Juarez Bridge.

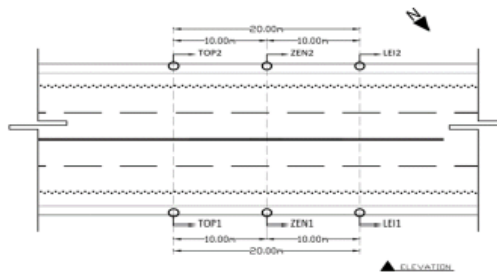


Figure 2. Location of GPS receivers.



Figure 3. Location of GPS base receivers.

Table 1. P_c and θ values for risk evaluation

Session	P_f			θ		
	± 1 cm	± 2 cm	± 3 cm	± 1 cm	± 2 cm	± 3 cm
Monday – 08:00-09:00	8.4205E-04	2.4359E-11	0.0000E+00	3.1409	6.5748	∞
Monday – 12:00-13:00	5.2005E-01	1.9825E-01	5.3628E-02	5.0268	8.4789	1.6106
Monday – 17:00-18:00	2.9596E-01	3.6594E-02	1.7162E-03	0.5360	1.7917	2.9261
Tuesday – 08:00-09:00	5.9581E-02	1.6472E-04	1.5893E-08	1.5583	3.5910	5.5313
Tuesday – 12:00-13:00	3.6841E-01	7.2031E-02	6.9678E-03	0.3361	1.4608	2.4589
Tuesday – 17:00-18:00	3.2237E-02	1.8446E-05	1.3242E-10	1.8489	4.1261	6.3181
Wednesday – 08:00-09:00	7.6270E-02	3.9187E-04	1.0477E-07	1.4306	3.3585	5.1907
Wednesday – 12:00-13:00	5.0920E-02	9.4496E-05	4.7284E-09	1.6360	3.7333	5.7402
Wednesday – 17:00-18:00	6.7026E-04	1.0251E-11	0.0000E+00	3.2072	6.7024	∞
Thursday – 08:00-09:00	1.0246E-02	2.8241E-07	1.3212E-14	2.3172	5.0029	7.6147
Thursday – 12:00-13:00	2.9129E-02	1.2802E-05	5.9418E-11	1.8937	4.2094	6.4408
Thursday – 17:00-18:00	2.5789E-04	2.7012E-13	1.1102E-16	3.4724	7.2148	8.2095
Friday – 08:00-09:00	3.1718E-02	1.7400E-05	1.1650E-10	1.8561	4.1395	6.3379
Friday – 12:00-13:00	1.0232E-01	1.0853E-03	9.5276E-07	1.2685	3.0658	4.7632
Friday – 17:00-18:00	3.8391E-03	7.3738E-09	0.0000E+00	2.6659	5.6645	∞
Saturday – 08:00-09:00	6.5325E-02	2.2776E-04	3.2193E-08	1.5115	3.5056	5.4062
Saturday – 12:00-13:00	3.3622E-01	5.4439E-02	3.9143E-03	0.4228	1.6033	2.6594
Saturday – 17:00-18:00	1.2337E-01	2.0592E-03	3.7943E-06	1.1583	2.8690	4.4765
Sunday – 08:00-09:00	2.3313E-03	1.1373E-09	0.0000E+00	2.8295	5.9769	∞
Sunday – 12:00-13:00	5.5412E-02	1.2749E-04	9.0894E-09	1.5945	3.6572	5.6285
Sunday – 17:00-18:00	1.6323E-01	5.2937E-03	2.8782E-05	0.9813	2.5560	4.0226

Recuperado de: https://www.researchgate.net/publication/333678255_Structural_Health_Monitoring_of_Bridges_using_GPS_Technology



Utility of GNSS Radio Occultation technique for tropopause height investigation over Egypt

Zhran, M., Mousa, A., Rabah, M. and Zeidan, Z., (2019). *NRIAG Journal of Astronomy and Geophysics*, 8 (1), 45-54.

Abstract

Global Navigation Satellite System (GNSS) Radio Occultation (RO) is an active limb sounding technique, where GNSS satellites transmitted signals passing through the atmosphere of the Earth and received by a GNSS receiver on low earth orbiter (LEO) satellite. RO provides accurate atmospheric refractivity profile. RO technique has been widely used to study the atmosphere of planets. This paper investigates the use of GNSS RO for tropopause height (TPH) estimation as one of the key climate parameters over Egypt. TPH is also very important in determining the wet delay in

GNSS analysis. Two years (2016 and 2017) of MetOP A and B satellites data are used. ROPP software package is used in the analysis. For validation of the results, RO-derived TPH is compared with European Centre for Medium-Range Weather Forecast (ECMWF) model as well as radiosonde (RS). Good agreement and high correlation are found between TPH from RO and ECMWF and RS on the other hand. TPH varies between 14 and 16 km over Egypt. It decreases with latitude and shows no clear trend with longitude. Tropopause temperature is found to increase with latitude.

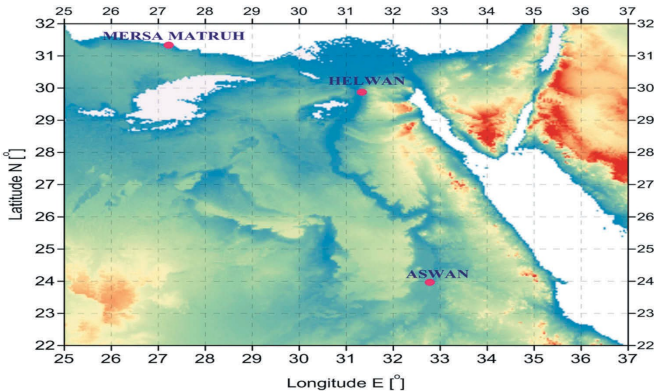


Figure 1. Map of radiosonde stations used in the validation.

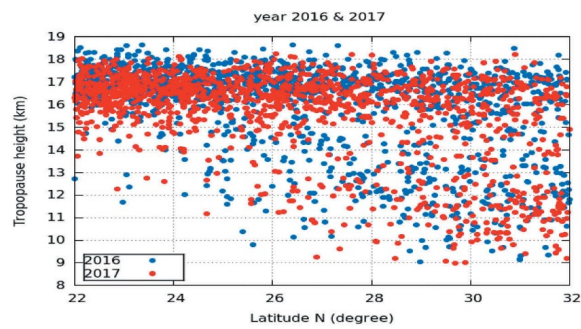


Figure 2. Tropopause height with latitude in 2016 and 2017.

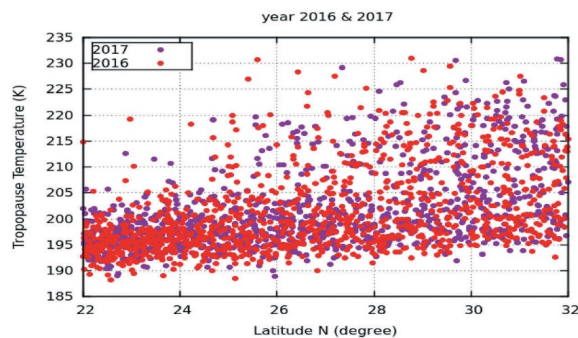


Figure 3. Tropopause temperature with latitude in 2016 and 2017.

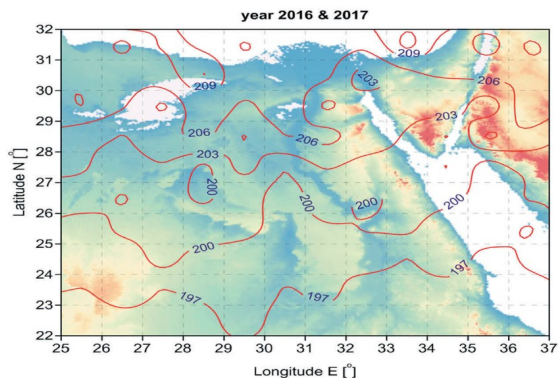


Figure 4. The zonal average tropopause temperature from the RO data.

Table 1. The used radiosonde stations for validation, including WMO identification number, latitude, longitude and elevation and number of co-located profiles.

Station Name	WMO ID	Lat [°N]	Long [°E]	Elev [m]	No. of co- located profiles
ASWAN	62,414	23.97	32.78	194	20
HELWAN	62,378	29.87	31.33	141	43
MERSA MATRUH	62,306	31.33	27.22	30	33



Shoreline monitoring by GNSS-PPP aiming to attendance the law 14.258/2010 from Pernambuco State, Brazil

Marques, H., Gonçalves, R., Araujo, A., Pereira, P. and Queiroz, H. (2019). *Bulletin of Geodetic Science*, 25 (2).

Abstract

The geodetic shoreline positioning has socioeconomic importance due to decision-making support related to the coastal zone. The Pernambuco state, Brazil, has established a state law no. 14.258/2010 sanctioned as part of Coastal Zone Management State Policy. The state act no. 42.010/2015 enacted the baseline information for Pernambuco shoreline. Considering that the shoreline mapping benefits from GNSS positioning using relative or absolute methods, the absolute PPP was the choice for legislation support. Therefore, the aim of this work is to depict about the Pernambuco state law and analyze the kinematic PPP accuracy applied to shoreline monitoring in order to attend

the state act. The relative GNSS method was adopted as reference to assess the PPP accuracy for the Pernambuco shoreline. The analyses for each sector involved approximately one hour of kinematic GNSS data and the results indicate horizontal positioning accuracy around 0.50 m after PPP convergence period. Several PPP re-initialization has been detected, however, points considered outliers are removed from the final product. For this reason, recommendations are provided to improve the positioning applied for coastal zone monitoring. Although, the carried out experiments shows that PPP can be adopted as a practical tool to support the Pernambuco Coastal Zone Management.



Figure 1. Kinematic Survey equipment (Receiver connected to the quadricycle)



Figure 2. Sectors A,B,C and D near RECF aiming the PPP accuracy análisis with data collecting time of approximately one hour.

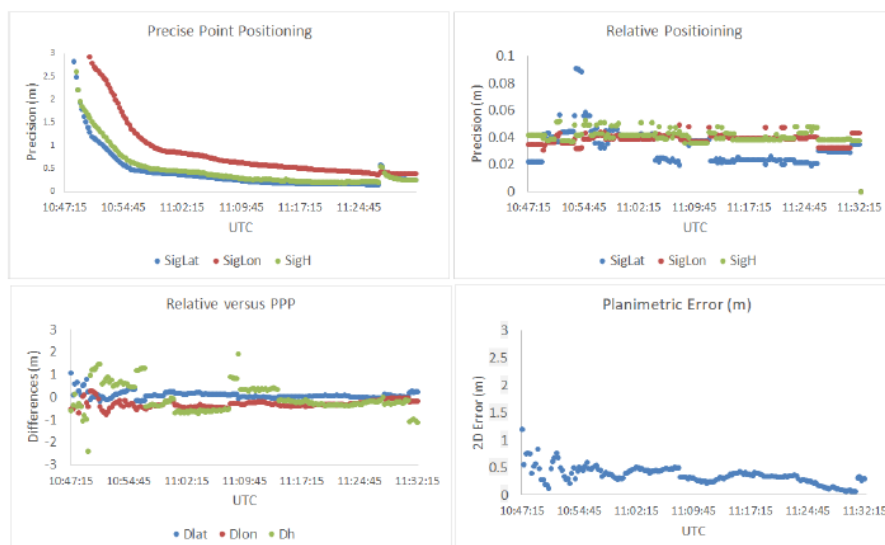


Figure 3. Time Series precisions and discrepancias between relative and PPP for the sector A.



Mapping Forest Landscape Multifunctionality Using Multicriteria Spatial Analysis

Navalho, I., Alegria, C., Roque, N. and Quinta-Nova, L., (2019). *Floresta e Ambiente*, 26 (2).

Abstract

This paper presents a GIS methodological approach for mapping forest landscape multifunctionality. The aims of the present study were: (1) to integrate and prioritize production and protection functions by multicriteria spatial analysis using the Analytic Hierarchy Process (AHP); and (2) to produce a multifunctionality map (e.g., production, protection, conservation and recreation) for a forest management unit. For this, a study area in inner Portugal occupied by forest and with an important protection area was selected. Based on maps for functions identified in the study area, it was possible to improve the scenic value and the biodiversity of the landscape to mitigate fire hazard and to diversify goods and services. The developed methodology is a key tool for producing maps for decision making support in integrated landscape planning and forest management.

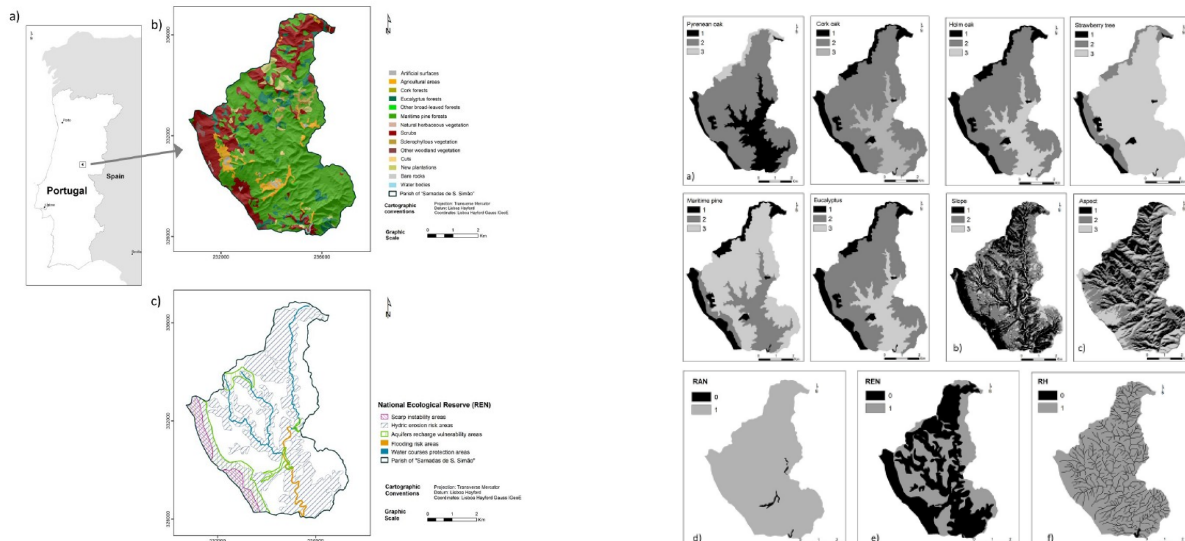


Figure 1. Study area: (a) geographical location of the study area (Sarnadas de S. Simão, municipality of Oleiros); (b) land cover map; and (c) National Ecological Reserve (REN).

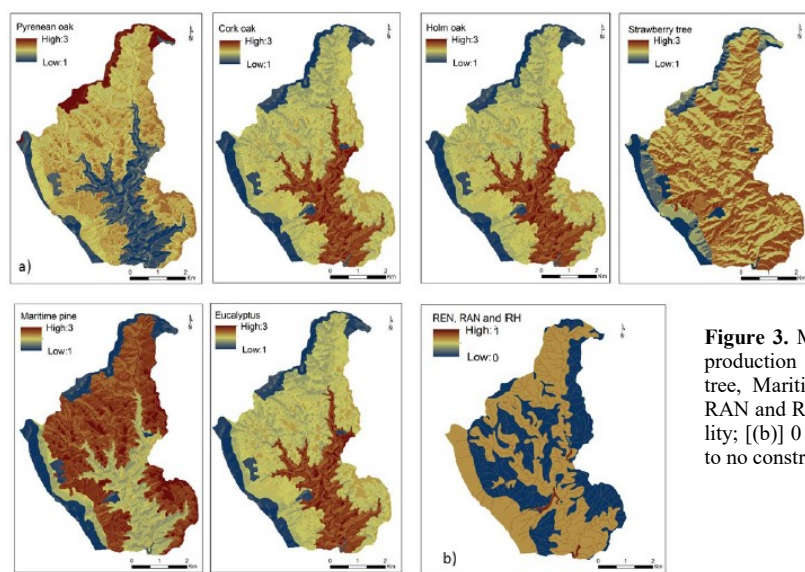


Figure 3. Maps of the production and protection obtained by AHP: (a) production function (Pyrenean oak, Cork oak, Holm oak, Strawberry tree, Maritime pine and Eucalyptus); (b) protection function (REN, RAN and RH). [(a)] 1 to 3 – Low and/or null suitability to high suitability; [(b)] 0 to 1 – Area with constraints (easements and/or restrictions) to no constraints.

Recuperado de: <https://doi.org/10.1590/2179-8087.070217>



Spatial analysis on tuberculosis and the network of primary health care

Leal, B., Mesquita, C., Rodrigues, I., Oliveira, L. and Caldas, R. (2019). *Revista Brasileira de Enfermagem REBEn*, 72(5), 1197-202.

Abstract

Objective: to analyze the spatial distribution of new cases of tuberculosis compared to the location of the Primary Healthcare Units that performed the compulsory notification. **Method:** ecological study conducted in Belém, Pará, with 5,294 new cases of tuberculosis notified to Sistema de Informação de Agravos de Notificação for the period from 2010 to 2014. The cases were georeferenced using the software applications ArcGis 10.2 and TerraView 4.2.2. The techniques of Kernel density and global Moran geostatistics were used. **Results:** the incidence of tuberculosis cases did not vary significantly between the years studied, however there was a variation in incidence between neighborhoods. Health units that exhibited higher number of notifications can suffer great influence of migration from nearby neighborhoods. **Conclusion:** the spatial dynamics of tuberculosis associated with health services allows to know the areas with increased risk of tuberculosis and the density of notifications of health units.

Recuperado de: <http://dx.doi.org/10.1590/0034-7167-2017-0897>

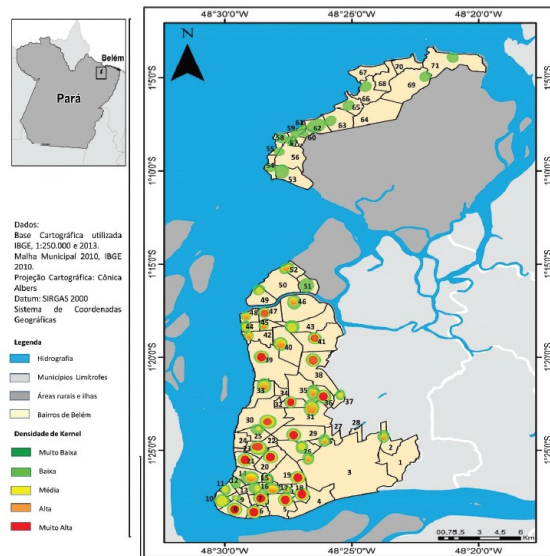


Figure 1. Kernel Density in the neighborhoods of Belem during the period of 2010-2014, Belem, Pará, Brazil

Land use and water quality in watersheds in the State of São Paulo, based on GIS and SWAT data

Barbosa, D., Gamero, M. and Cassia, A., (2019). *Ambiente & Água—An Interdisciplinary Journal of Applied Science*, 14 (5).

Abstract

Land use influences the quality and availability of water resources, but Brazil has made little progress in integrated watershed management. This study therefore applied geoprocessing for land-use classification and evaluated the impact on the hydrological balance in order to contribute to the integrated management of water resources. Using GIS tools, two drainage areas from the water catchment points of two municipalities, Santa Cruz das Palmeiras and Piedade, were delimited; land-use mapping was carried out using the supervised classification method of satellite images, and the SWAT model was applied for hydrological simulation. The methods used were appropriate. The surface runoff was related to the absence of vegetation and the predominance of exposed soil. The relationship between land use/land cover and the hydrological balance was evidenced, especially the impact of agricultural activities and the lack of natural vegetation in the surface runoff.

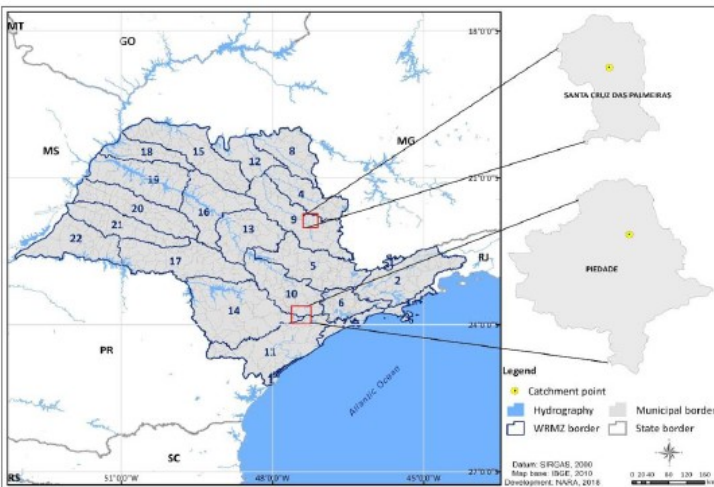


Figure 1. Location of the studied municipalities and the Water Resources Management Zones (WRMZs) within the state of São Paulo.

Recuperado de: <http://dx.doi.org/10.4136/ambi-agua.2325>



Cleaning radio interferometric images using spherical decomposition

Skipper, C., Scaife, A. and McEwen, J., (2019). *Astronomy and Computing*, 29.

Abstract

The deconvolution, or cleaning, of radio interferometric images often involves computing model visibilities from a list of clean components, in order that the contribution from the model can be subtracted from the observed visibilities. This step is normally performed using a forward fast Fourier transform (FFT), followed by a ‘degridding’ step that interpolates over the uv plane to construct the model visibilities. An alternative approach is to calculate the model visibilities directly by summing over all the members of the clean component list, which is a more accurate method that can also be much slower. However, if the clean components are used to construct a model image on the surface of the celestial sphere then the model visibilities can be generated directly from the wavelet coefficients, and the sparsity of the model means that most of these coefficients are zero, and can be ignored. We have constructed a prototype imager that uses a spherical-wavelet representation of the model image to generate model visibilities during each major cycle, and find empirically that the execution time scales with the wavelet resolution level, J , as $O(1.07J)$, and with the number of distinct clean components, NC , as $O(NC)$. The prototype organises the wavelet coefficients into a tree structure, and does not store or process the zero wavelet coefficients.

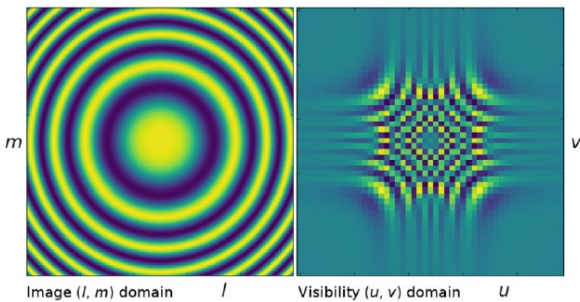


Figure 1. Example w-kernel for degridding, $K_{ju,v}$, shown in the image domain (left panel) and uv domain (right panel).

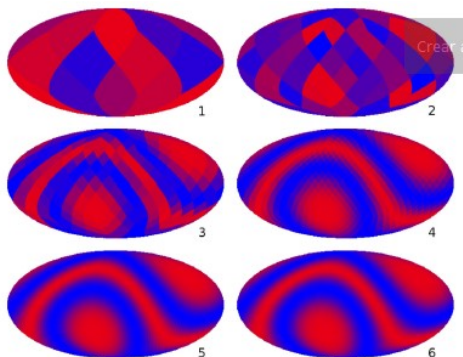


Figure 2. Scaling coefficients, $n_j k(B)$, of the plane-wave function, $F P(\zeta, B)$, for the first six resolution levels ($j = 1$ to $j = 6$), shown over the whole unit two-sphere in Mollweide projection.

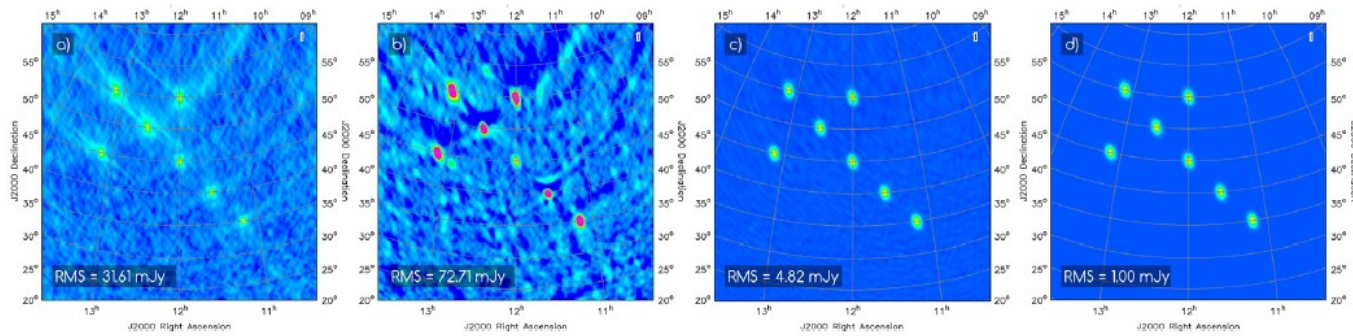


Figure 3. (a) Dirty image from a wide-field simulated measurement set, generated using 64 w-planes. (b) Image cleaned with 700 CLEAN iterations over four major cycles using a conventional CLEAN algorithm that includes a forward FFT and degridding. For degridding we used only the anti-aliasing kernel, whereas both the anti-aliasing kernel and w-kernel (64 w-planes) were used during gridding. (c) Image cleaned with 700 CLEAN iterations over four major cycles using a conventional degridding algorithm to calculate the model visibilities. We have used w-projection, with 64 w-planes, in both the forward and inverse directions. (d) The same measurement set, cleaned with 580 CLEAN iterations over four major cycles, and using 64 w-planes while gridding and the wavelet clean algorithm in place of degridding.



BeamModelTester: Software framework for testing radio telescope beams

Creanel, O. and Carozzi, T., (2019). *Astronomy and Computing*, 28.

Abstract

The flux, polarimetric and spectral response of phased array radio telescopes with no moving parts such as LOFAR is known to vary considerably with orientation of the source to the receivers. Calibration models exist for this dependency such as those that are used in the LOFAR pipeline. Presented here is a system for comparing the predicted outputs from any given model with the results of an observation. In this paper, a sample observation of a bright source, Cassiopeia A, is used to demonstrate the software in operation, by providing an observation and a model of that observation which can be compared with one another. The package presented here is flexible to allow it to be used with other models and sources. The system operates by first calculating

the predictions of the model and the results of an observation of linear fluxes and Stokes parameters separately. The model and observed values are then joined using the variables common to both, time and frequency. Normalisation and RFI excision are carried out and the differences between the prediction and the observation are calculated. A wide selection of 2-, 3- and 4-dimensional plots is generated to illustrate the dependence of the model and the observation as well as the difference between them on independent parameters time, frequency, altitude and azimuth. Thus, beamModelTester provides a framework by which it is possible to calibrate and propose refinements to models and to compare models with one another.

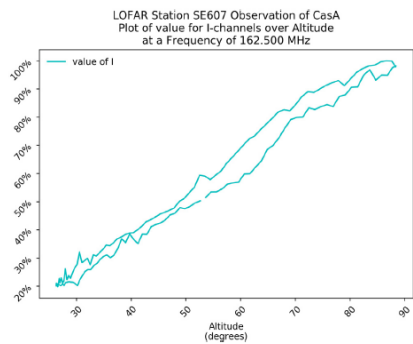


Figure 1. A plot of observed flux (Stokes I) from CasA against Altitude as observed with LOFAR Station SE607 HBA at 162.5MHz over 24 h. Plot (including title and axis labels) automatically generated using beamModelTester.

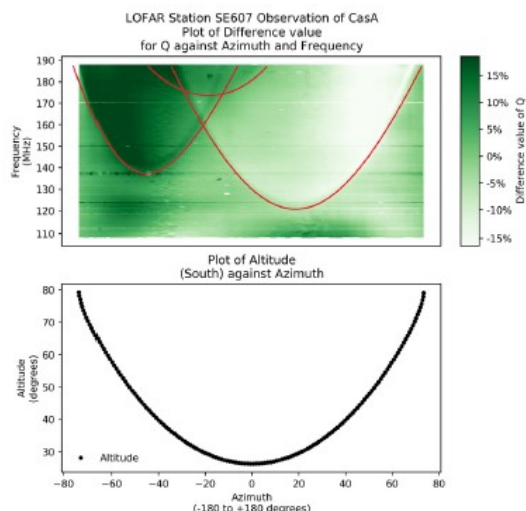


Figure 2. (top) A plot of the difference between observed and model of linear polarisation (Stokes Q) against Azimuth and Frequency. (bottom) A plot of Altitude against Azimuth at the corresponding times of this observation to indicate the variation in two independent variables.

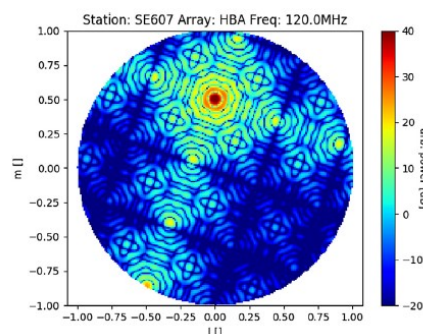


Figure 3. (a) Orthographic projection model of the Array Factor of LOFAR HBA station SE607 at 120MHz. Note the extensive sidelobe patterns reaching all the way to the horizon. Plot generated using dreamBeam.

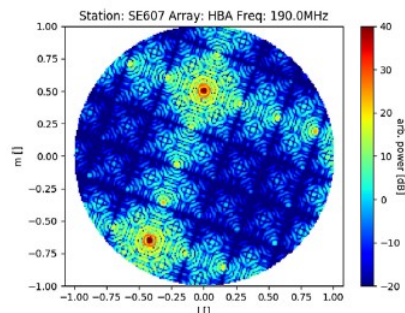


Figure 4. Orthographic projection model of the beampattern of LOFAR HBA station SE607 at 190MHz. Note the differences in the beampattern from that shown in Fig. 3. In particular, note the narrower spacing of the fringes and the strong local maximum located close to the horizon. Plot generated using dreamBeam.



NOTICIAS

Lanzado el satélite GaoFen-10

El 31 de agosto de 2016, un fallo de lanzamiento provocó la pérdida del satélite chino GaoFen-10. El 4 de octubre de 2019, un cohete CZ-4C lanzaba desde la base de Taiyuan a su sustituto, que fue colocado en una órbita polar heliosincrónica de unos 600 km de altitud.

El vehículo, que partió a las 18:51 UTC, recibió el mismo nombre que su antecesor una vez en el espacio. Los GaoFen están dedicados a la observación de la superfi-

cie terrestre, en el marco de un programa civil.

Las características exactas del satélite no se conocen, solo se supone que está equipado con una cámara de alta resolución. El anuncio oficial habla de gestión urbana y agrícola, prevención de desastres naturales, etc. Sin embargo, la escasez de detalles sugiere que podría tener también aplicaciones militares.



Noticia completa en: <https://noticiasdelaciencia.com/art/34601/lanzado-el-satelite-gaofen-10>

Una nueva misión de la Agencia Espacial Europea ayudará a conocer mejor el clima



La misión FORUM (Far-infrared Outgoing Radiation Understanding and Monitoring, o Comprensión y Vigilancia de la Radiación Saliente en el Infrarrojo Lejano) aportará un tipo de medición crucial para ayudarnos a entender el clima cambiante de nuestro planeta.

Las mediciones de este nuevo satélite incrementarán la exactitud de las valoraciones sobre el cambio climático que se utilizarán como base para las futuras decisiones políticas.

FORUM registrará la radiación en el infrarrojo lejano que la Tierra emite al espacio, yendo más allá de las porciones del espectro de infrarrojos que se miden en la actualidad. Estas mediciones ayudarán a estudiar el balance de radiación terrestre: el equilibrio entre la radiación entrante, procedente en su mayor medida del Sol a longitudes de onda cortas, y la radiación saliente, que es una combinación de la radiación reflejada del Sol y la radiación emitida por el sistema terrestre, en gran parte a longitudes de onda más largas.

Noticia completa en: <https://noticiasdelaciencia.com/art/34496/una-nueva-mision-de-la-agencia-espacial-europea-ayudara-a-conocer-mejor-el-clima>

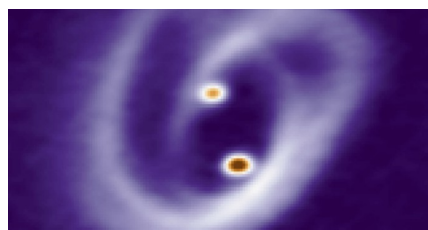
Observan por primera vez cómo se forman las estrellas gemelas

Científicos de varios países han observado por primera vez cómo se forman las estrellas gemelas, o sistemas estelares binarios, que son la forma más común en que las estrellas se presentan en el universo. El resultado, publicado en *Science*, muestra imágenes de alta resolución obtenidas con el instrumento ALMA (Atacama Large Millimetre/submillimetre Array).

Los astrónomos han observado el sistema [BHB2007] 11, el miembro más joven de un pequeño grupo de jóvenes objetos estelares en la nebulosa oscura Barnard 59, que forma parte de la nube

de polvo y gas llamada la Nebulosa de la Pipa. Mientras que las observaciones anteriores mostraban una envoltura giratoria y en colapso alrededor de un disco circumbinario, ahora, las nuevas observaciones también revelan su estructura interna.

“Vemos dos fuentes compactas, que interpretamos como discos circunestelares alrededor de las dos jóvenes estrellas”, explica Felipe Alves, que actualmente investiga en Max Planck Institute for Extraterrestrial Physics (MPE). Las estrellas crecen al extraer materia de estos discos.



Noticia completa en: <https://noticiasdelaciencia.com/art/33988/astrofisico-gaditano-realiza-un-nuevo-descubrimiento-sobre-como-se-forman-las-estrellas>



UNIVERSIDAD AUTÓNOMA DE SINALOA
FACULTAD DE CIENCIAS DE LA TIERRA Y EL ESPACIO



CONGRESOS



International Conference on Geospatial Information Sciences 2019

Sede: CentroGeo, Laboratorio de Geointeligencia Nacional, Mérida, Yucatán

Fecha: 22 al 25 de octubre

Sitio web del congreso: <http://igisc.org/>



Reunión Anual de la Unión Geofísica Mexicana 2019

Sede: hotel Sheraton Buganvillas en Puerto Vallarta, Jalisco

Fecha: 27 de octubre al 1 de noviembre

Sitio web del congreso: <https://raugm.org.mx/>



PROGRAMA DE CONFERENCIAS Y TALLERES PARA LA FORMACIÓN INTEGRAL Y PROFESIONAL 2019-2020 I

Conferencia/Taller	Imparte	Lugar y fecha
Taller: Valores Universitarios	BIENESTAR UNIVERSITARIO	Aula 7 Martes 01 de octubre 8:30 h – 9:30 h.
Taller: Formación de equipos de trabajo	DGVRI	Aula 1 Martes 01 de octubre 14:20 –15:30 h.
Taller: Batimetría (Teoría)	Ing. Iván Escalante Mondaca	Aula 4 Martes 01 de octubre 10:00 h – 13:00 h.
Taller: Buscadores de empleo	DGVRI	Centro de cómputo Jueves 03 de octubre 14:20 –15:30 h.
Taller: Batimetría (Práctica)	Ing. Iván Escalante Mondaca	Presa Sanalona Jueves 03 de octubre 8:00 h.
1era. Sesión Seminario: “Proceso de Incubación”	DGVRI	Auditorio Jueves 03 de octubre 12:40 –14:00 h.
Taller: Valores Universitarios	BIENESTAR UNIVERSITARIO	Auditorio Viernes 04 de octubre 13:00 –14:00 h.
Taller: Batimetría (Procesamiento de datos)	Ing. Iván Escalante Mondaca	Aula 4 Martes 08 de octubre 10:00 –13:00 h.

SE OTORGARÁ 1 CRÉDITO POR CADA 3 EVENTOS.



Conferencia/Taller	Imparte	Lugar y fecha
Conferencia: “Raíces Volcánicas”	Dra. Xóchitl Torres Carrillo	Auditorio Martes 8 de octubre 10:00 h – 11:00 h.
Actividad: Desarrollo Sostenible (Visita a la reserva)	M.C. Edgar Benjamín López Camacho	Cosalá 10 y 11 de octubre
Conferencia: Espacio 100% libres de humo de tabaco	BIENESTAR UNIVERSITARIO	Auditorio Martes 15 de octubre 13:00 h – 14:00 h.
Taller ejecutivo Mapa Digital de México para escritorio versión 6.1.	INEGI	Centro de cómputo Miércoles 16 de octubre 11:20 h – 13:20 h.
Conferencia: “De la Tierra a la Luna: La historia del Apollo 11”	Dr. Christopher Añorve Solano	Auditorio Miércoles 16 de octubre 14:20 h.
2da. Sesión Seminario: “Proceso de incubación”	DGVRI	Auditorio Jueves 17 de octubre 12:40 h – 15:40 h.
Taller ejecutivo Mapa Digital de México para escritorio versión 6.1.	INEGI	Centro de cómputo Viernes 18 de octubre 12:20 h – 14:20 h.
Taller: “Computación Gráfica y Científica con Python”	Dr. Christopher Añorve Solano	Centro de cómputo Martes 22 y jueves 24 de octubre 11:00 h – 14:00 h.

SE OTORGARÁ 1 CRÉDITO POR CADA 3 EVENTOS.



Conferencia/Taller	Imparte	Lugar y fecha
Taller: “Fotogrametría con Drones”	Dr. Juan Martín Aguilar Villegas	Centro de cómputo Lunes 28 y Martes 29 de octubre 11:00 h – 14:00 h.
3era. Sesión Seminario - “Proceso de incubación”	DGVRI	Auditorio Jueves 31 de octubre 12:40 h – 15:40 h.
Conferencia: Observaciones GPS de Alta Frecuencia (High Rate) y datos sismológicos para monitorear la deformación cosísmica de la Península de Baja California, México	Ing. Carlos Ramón Moraila Valenzuela	Auditorio Lunes 4 de noviembre 10:00 h – 11:20 h.
Taller: Valores Universitarios	BIENESTAR UNIVERSITARIO	Aula 5 Miércoles 6 de noviembre 11:30h– 12:30 h.
Taller: “Uso y Manejo de Telescopios”	C. Sebastián Carrazco Gaxiola	Auditorio Lunes 11 de noviembre 17:20 h – 18:40 h.
Taller: Valores Universitarios	BIENESTAR UNIVERSITARIO	Aula 6 Miércoles 13 de noviembre 13:00 h – 14:00 h.
Curso-Taller: “Desarrollo de Interfaces gráficas con Python 3”	L.I. Jesús Abel Cota Dimas	Centro de cómputo Martes 19 de noviembre 10:00 h – 13:00 h.

SE OTORGARÁ 1 CRÉDITO POR CADA 3 EVENTOS.



Conferencia/Taller	Imparte	Lugar y fecha
Conferencia: “Competencias que demanda el mundo laboral”	DGVRI	Aula 4 Viernes 22 de noviembre 8:00 h – 9:30 h
Conferencia: “Recomendaciones para una buena entrevista profesional”	DGVRI	Aula 3 Lunes 25 de noviembre 17:30 h – 18:30 h.
Taller: Análisis de información obtenida de las mediciones GPS	Dr. Rosendo Romero Andrade	Martes 26 de noviembre 11:00 h – 13:00 h.
Conferencia: “Gases de efecto invernadero: Cambio Climático”	Dr. Sergio Monjardín Armenta	Auditorio Miércoles 27 de noviembre 13:00 h – 14:00 h
Taller: Análisis de información obtenidas de las Mediciones GPS	Dr. Rosendo Romero Andrade	Jueves 28 de noviembre 11:00 h – 13:00 h.

SE OTORGARÁ 1 CRÉDITO POR CADA 3 EVENTOS.